A Robust Dual-Vector Model Predictive Current Control for PMSM Drives

Lu Xu[1] iD, Xiaoguang Zhang[1] iD

[1] North China University of Technology, China

[2] North China University of Technology, China

Corresponding author: Xiaoguang Zhang, zxg@ncut.edu.cne

Speaker: Lu Xu, xvlu@mail.ncut.edu.cn

Abstract

Given the high dependence of traditional model predictive current control (MPCC) methods on the accuracy of motor parameters, this paper proposes a robust dual-vector MPCC (DV-MPCC) method. In this control strategy, separate value functions are designed for the d-axis and q-axis based on sampled information. Subsequently, through the computation of these value functions and rolling optimization, the actual parameters of the motor are estimated. Simultaneously, this estimation information is used to dynamically adjust the predictive model in real-time, thereby achieving strong parameter robustness in control performance. Finally, simulation experiments are conducted to validate the effectiveness of the proposed method in reducing sensitivity to DV-MPCC parameters.

1 Introduction

Currently, compared with other motors, Permanent Magnet Synchronous Motors (PMSMs) are widely used in high-performance drive applications due to their high power density, fast dynamic response, and low maintenance cost [1-3]. However, PMSMs are complex nonlinear control systems, and achieving satisfactory control with typical proportional-integral control is difficult. Therefore, new control methods such as fuzzy control [4], sliding-mode control [5], adaptive control [6], and model predictive control (MPC) [7-8] have emerged. Among these, with the advancement of modern control theory and the development of chip processing technology, MPC has been extensively studied by numerous researchers due to its advantages of simple modeling and ability to handle nonlinear constraint problems effectively [9-11].

Furthermore, to enhance the control performance of the traditional MPC method, researchers have proposed the duty cycle-based MPC method and the dual vector-based MPC method [12-13]. The duty cycle MPC method employs one zero vector and one non-zero vector per control cycle, enabling flexible adjustment of the non-zero vector's amplitude. In contrast, the dual vector-based MPC method utilizes any two voltage vectors (VVs) per control cycle. This method provides greater freedom and flexibility by combining these VVs, thereby effectively reducing current ripple and improving system control performance.

However, the MPC method relies on a mathematical model that includes motor parameters, such as resistance, inductance, and magnet chain characteristics. Consequently, any discrepancies in these motor parameters will lead to errors between the predicted and actual values. Inaccuracies in the prediction model can result in the selection of suboptimal VVs, thereby impacting the control performance of the system [14-15]. This underscores the critical dependence of MPC control accuracy on the precision of motor parameters. Furthermore, compared to single-vector MPC, dual-vector MPC involves an additional step of calculating the time allocation for VVs, which also requires precise motor parameters. Therefore, dual-vector MPC demands even higher parameter accuracy

In order to enhance the parameter robustness of dual-vector model predictive current control (DV-MPCC), this paper, a dual vector model predictive current control method with robust characteristics is proposed. This method calculates parameter information in the dq-axes separately based on real-time motor sampling data and performs real-time correction of the prediction model. It achieves accurate parameter estimation with strong robustness using existing information, without requiring any prior knowledge of motor parameters.

The structure of this paper is organized as follows: Section II introduces the traditional DV-MPCC. Section III elaborates on the core concepts and control strategies of the proposed robust method. Section IV validates the effectiveness of the proposed robust

method through simulations. Finally, Section V presents the conclusion.

2 Mathematical Model of PMSM

First of all, the control object in this paper is a surface mounted PMSM (SPMSM), which is inherently characterized by equal inductance values in the d-axis and the q-axis, i.e., $L_d = L_q = L$. Therefore, the SPMSM stator current equation of state in the rotating coordinate system can be expressed as

$$\begin{cases} \dfrac{\mathrm{d}i_d}{\mathrm{d}t} = \dfrac{1}{L}(u_d - Ri_d + \omega_e L i_q) \\ \dfrac{\mathrm{d}i_q}{\mathrm{d}t} = \dfrac{1}{L}(u_q - Ri_q - \omega_e L i_d - \omega_e \psi_f) \end{cases} \quad (1)$$

where u_d, u_q, i_d, i_q represents the voltage and current components of the dq-axes. R, L, ψ_f and ω_e denote stator resistance, inductance, permanent magnet chain and electrical angular velocity respectively.

Then, following the first-order Eulerian discretization method, the predicted current at $(k+1)^{\mathrm{th}}$ instant can be expressed as

$$\begin{cases} i_d^p(k+1) = i_d(k) - \dfrac{T_s}{L} A_d(k) + \omega_e T_s i_q(k) \\ i_q^p(k+1) = i_q(k) - \dfrac{T_s}{L} A_q(k) - \omega_e T_s i_d(k) \end{cases} \quad (2)$$

where $\begin{cases} A_d(k) = Ri_d(k) - u_d(k) \\ A_q(k) = Ri_q(k) - u_q(k) + \omega_e \psi_f \end{cases}$ and T_s is the control period in the system.

3 Traditional DV-MPCC Method

The controlled surface mounted PMSM (SPMSM) in the article is realized by utilizing a two-level voltage source inverter (2L-VSI), and the topology is depicted in Fig. 1.
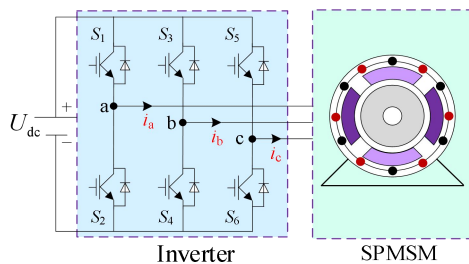

Fig. 1. Topology of SPMSM system.

Furthermore, the switching states produced by the 2L-VSI can be portrayed as

$$S = [S_{a1} \quad S_{b1} \quad S_{c1}]^T \quad (2)$$

where S_{a1}, S_{b1}, S_{c1} denote the phase change state of each phase in the three upper bridge arms of

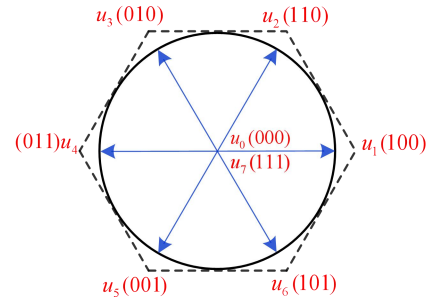the inverter, respectively. And the correlation between the switching state and VV is depicted in Fig. 2.

Fig. 2. The relationship between the switching state and voltage vector in a 2L-VSI.

The selection of the first and second VVs in traditional DV-MPCC (T-DV-MPCC) is similar to that in single-vector MPCC, but it involves a time allocation calculation for two VVs. Therefore, the combined effect of the first and second VVs must be carefully considered. Once the first VV is determined, it is combined with the remaining seven VVs, and the time allocation calculation is performed simultaneously. Finally, the optimal synthesized VV is obtained through a rolling optimization search. This synthesized VV can be expressed as

$$u_s^s(k) = \frac{[t_1 u_{s1}(k) + t_2 u_{s2}(k)]}{T_s} \quad (4)$$

Where t_1 and t_2 denote the timings of the first and second optimal VV, respectively, with $t_2 = T - t_1$. The determination of the operation times of the VVs within one sampling period is calculated according to the deadbeat control principle for the dq-axes currents [16], specifically,

$$i_{qs}(k+1) = i_{qs}(k) + K_{q1} t_1 + K_{q2} t_2 = i_q^* \quad (5)$$

where i_q^* denotes the reference current of q-axis. K_{q1} and K_{q2} denote the current slopes of the q-axis generated by the effects of the two VVs, which can be represented as

$$\begin{cases} K_{q1} = \mathrm{d}i_{q1}/\mathrm{d}t = K_{q0} + u_{q1}/L \\ K_{q2} = \mathrm{d}i_{q2}/\mathrm{d}t = K_{q0} + u_{q2}/L \\ K_{q0} = \mathrm{d}i_{q0}/\mathrm{d}t = -R \cdot i_q/L - \omega_e i_d - \omega_e \psi_f/L \end{cases} \quad (6)$$

According to (5), the timing of the first optimal VV can be represented as

$$t_1 = \frac{\left[i_q^* - i_{qs}(k) - K_{q2} \cdot T_s\right]\left(K_{q1} - K_{q2}\right)}{\left(K_{q1} - K_{q2}\right)^2}. \quad (7)$$

Ultimately, using cost function (8) as the evaluation criterion, the predicted currents with the synthesized VVs are incorporated into value function (8) for assessment and decision-making. The optimal vector

combination that minimizes the current error is then selected.

$$J = \left[i_d^* - i_{ds}^p(k+1) \right]^2 + \left[i_q^* - i_{qs}^p(k+1) \right]^2 \qquad (8)$$

where $i_d^s(k+1)$ and $i_q^s(k+1)$ denote the predicted current after the synthesis of the two VVs.

The control framework of T-DV-MPCC with one-step delay compensation is shown in Fig.3.
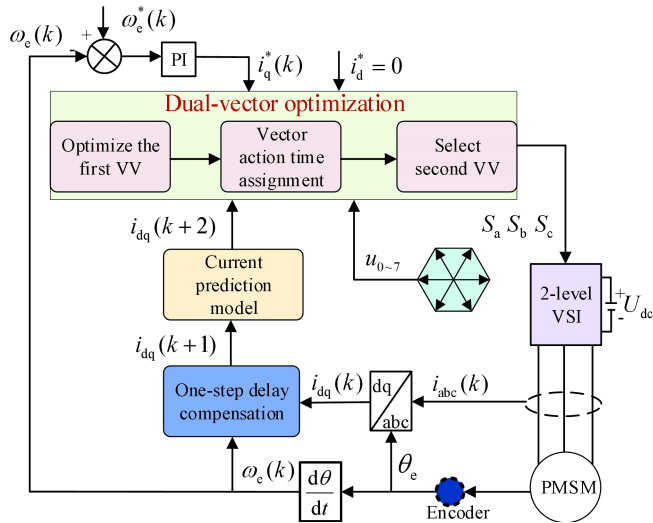

Fig. 3. Control schematic diagram of traditional DV-MPCC.

4 Proposed Robust Method

4.1 Establishment of a robust prediction model

Since the paper adopts control based on $i_d = 0$, and $T \cdot R / L \cdot i_d^*$ is much less than 1, this part can be ignored. At this point, prediction model (2) can be updated as

$$\begin{cases} i_{dx}^p(k+1) = i_d(k) + \dfrac{T}{L} u_d(k) + T\omega_e i_q(k) \\[2mm] i_{qx}^p(k+1) = \left(1 - \dfrac{TR}{L}\right) i_q(k) + \dfrac{T}{L} u_q(k) - T\omega_e i_d(k) - \dfrac{T\psi_f\omega_e}{L} \qquad (x=1,2) \\[2mm] \qquad = i_q(k) + \dfrac{T}{L} u_q(k) - T\omega_e i_d(k) - \dfrac{T\omega_e}{L}\left(\psi_f + \dfrac{Ri_q(k)}{\omega_e}\right) \end{cases} \qquad (9)$$

where x=1 denotes the selected first VV and x=2 denotes the selected second VV.

From (8), it is evident that the d-axis prediction model only includes the inductance parameter, while the q-axis prediction model incorporates resistance, inductance, and magnet chain parameters. To remove motor parameter information from the prediction model, this paper employs *T/L* and $\psi_f + R \cdot i_q / \omega_e$ as two consolidated parameters for real-time computation,

thereby obtaining accurate motor parameter information during operation. Consequently, the updated prediction model is formulated as

$$\begin{cases} i_{dx}^p(k+1) = i_d(k) + Xu_d(k) + T\omega_e i_q(k) \\[2mm] i_{qx}^p(k+1) = i_q(k) + Xu_q(k) - T\omega_e i_d(k) - \omega_e XY \end{cases} \qquad (10)$$

where $X=T/L$, $Y = \psi_f + Ri_q / \omega_e$.

4.2 Motor Parameter Estimation

Given that the aggregate parameter *X*, containing inductance information, appears exclusively in the d-axis prediction model, this paper employs *X* as a performance index for designing the d-axis value function to accurately determine *T/L* during motor operation. Similarly, the aggregate parameter *Y*, which encompasses magnetic chain and resistance information, appears only in the q-axis prediction model. This paper also utilizes *Y* as a performance index to construct the q-axis value function. The specific steps are outlined as follows.

First, the value functions for the d-axis and q-axis are formulated as follows

$$CF_1 = \underbrace{\left[i_{ds}^p(k+1) - i_d(k+1) \right]^2}_{term1} + H_d \underbrace{\left[X(k+1) - X(k) \right]^2}_{term2} \quad (11)$$

$$CF_2 = \underbrace{\left[i_{qs}^p(k+1) - i_q(k+1) \right]^2}_{term1} + H_q \underbrace{\left[Y(k+1) - Y(k) \right]^2}_{term2} \quad (12)$$

where H_{dq} denotes the weighting coefficient between the dq-axis current and the aggregate parameters *X*, *Y*. $i_{ds}^p(k+1)$ and $i_{qs}^p(k+1)$ denote the d-axis and q-axis currents under the action of the synthesized VV, respectively.

From the two value functions, it can be observed that as *term*1 approaches 0, it indicates minimal current error. As *term*2 approaches 0, it signifies that the calculated information of the aggregate parameter sets at the two moments is very close. If both of these conditions are satisfied simultaneously, the most suitable *X* and *Y* can be obtained. Therefore, it is necessary to compute the partial derivatives of *X*(k+1) and *Y*(k+1) in (10) and (11) to find the minimum values of *CF*₁ and *CF*₂ that satisfy these conditions, which can be formulated as

$$\frac{\partial CF_1}{\partial X(k+1)} = 2\left[i_d^p(k+1) - i_d(k+1) \right] u_d(k) \\ + 2H_d \left[X(k+1) - X(k) \right] \qquad (13)$$

$$\frac{\partial CF_2}{\partial Y(k+1)} = 2\left[i_q^p(k+1) - i_q(k+1) \right]\left[-X(k)\omega_e \right] \\ + 2H_q \left[Y(k+1) - Y(k) \right]. \qquad (14)$$

Let (13) and (14) be equal to 0. In this case, the optimal values of $X(k+1)$ and $Y(k+1)$ are obtained and expressed as

$$X(k+1) = X(k) - \frac{u_{\mathrm{d}}(k)\left[i_{\mathrm{ds}}^{\mathrm{p}}(k+1) - i_{\mathrm{d}}(k+1)\right]}{H_{\mathrm{d}}} \qquad (15)$$

$$Y(k+1) = Y(k) + \frac{\left[i_{\mathrm{qs}}^{\mathrm{p}}(k+1) - i_{\mathrm{q}}(k+1)\right]\left[X(k)\omega_{\mathrm{e}}\right]}{H_{\mathrm{q}}} \qquad (16)$$

Since the predicted and sampled currents at moment $(k+1)^{\mathrm{th}}$ instant are unknown, it is necessary to shift the moments in (12), (13) forward by onecontrol period, i.e.

$$X(k) = X(k-1) - \frac{u_{\mathrm{d}}(k-1)\left[i_{\mathrm{ds}}^{\mathrm{p}}(k) - i_{\mathrm{d}}(k)\right]}{H_{\mathrm{d}}} \qquad (17)$$

$$Y(k) = Y(k-1) + \frac{\left[i_{\mathrm{qs}}^{\mathrm{p}}(k) - i_{\mathrm{q}}(k)\right]\left[X(k-1)\omega_{\mathrm{e}}\right]}{H_{\mathrm{q}}} \qquad (18)$$

Similarly, the slopes K_{q1} and K_{q2} in the time calculation can also be expressed using the estimated information as

$$\begin{cases} K_{\mathrm{q1}} = \mathrm{d}i_{\mathrm{q1}}/\mathrm{d}t = K_{\mathrm{q0}} + Xu_{\mathrm{q1}}/T \\ K_{\mathrm{q0}} = \mathrm{d}i_{\mathrm{q0}}/\mathrm{d}t = -Ri_{\mathrm{q}}/L - \omega_{\mathrm{e}}i_{\mathrm{d}} - \psi_{\mathrm{f}} \\ \qquad = -\omega i_{\mathrm{d}} - \omega_{\mathrm{e}} XY/T \end{cases} \qquad (19)$$

The control framework of proposed robust DV-MPCC with one-step delay compensation is shown in Fig. 4.
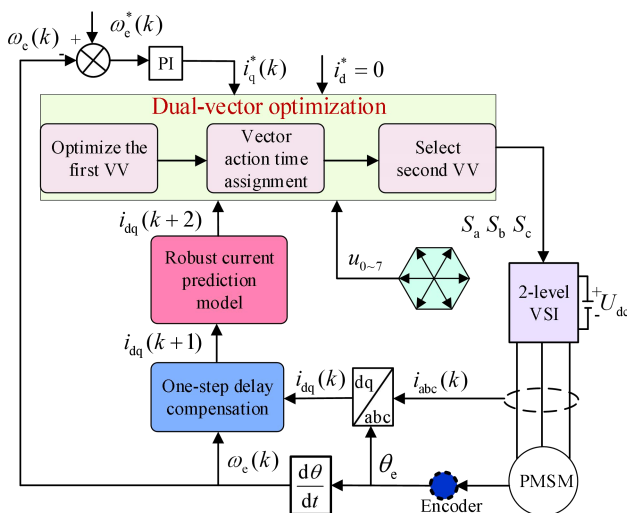

Fig. 4. Control schematic diagram of the proposed robust method.

5 Simulation Experiment

In order to verify the effectiveness of the methods proposed in this paper in terms of robust performance , relevant simulation experiments are designed in this section. The parameters of the control system are shown in Table I.

TABLE I
PARAMETERS OF SPMSM

Symbol	Value	Symbol	Value
U_{dc} (V)	310	P_{N} (kW)	1.25
R (Ω)	3.18	T_{N} (N·m)	5
L (mH)	8.5	n_{N} (r/min)	2000
ψ_{f} (Wb)	0.325	p	2

As demonstrated in Figs. 5-6, this section assesses and validates the steady-state performance of the proposed methods. Initially, Fig. 5 presents the steady-state results of the T-DV-MPCC and the proposed robust method at a torque of 4 N-m and a speed of 500 r/min. Under these conditions, the total harmonic distortion (THD) of the T-DV-MPCC current is 3.87%, with dq-axis current ripples of 0.70 A and 0.35 A. In comparison, the proposed robust method achieves a phase current THD of 3.80% and dq-axis current ripples of 0.70 A and 0.34 A.

Subsequently, the performance of the proposed robust method is evaluated with a constant load torque while increasing the speed to 2000 r/min. It is observed that the robust method performs comparably to the T-DV-MPCC, maintaining a similar level of control. This indicates that the proposed method exhibits robust performance and can effectively mitigate the parameter sensitivity issue associated with the T-DV-MPCC method.
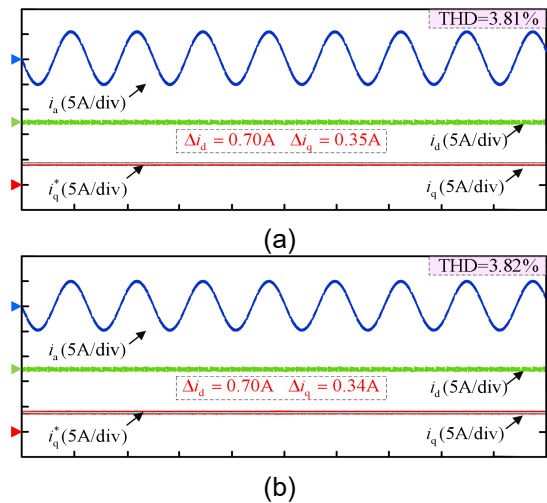

Fig. 5. Simulation results at rated load and speed of 500 r/min, (a) T-DV-MPCC method, (b) Proposed robust method.
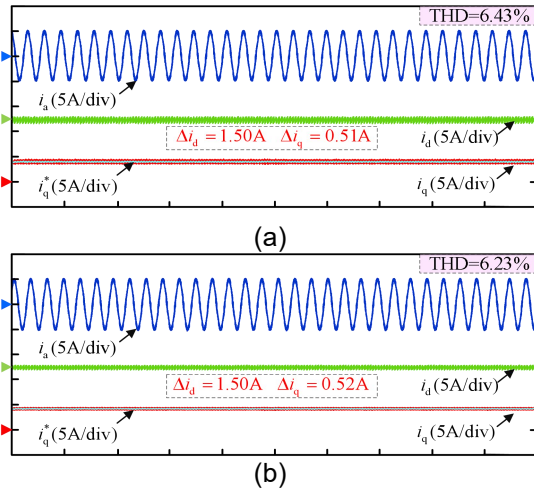
Fig. 6. Simulation results at rated load and speed of 2000 r/min, (a) T-DV-MPCC method, (b) Proposed robust method.

The above experimental results show that the proposed robust method can maintain a control performance comparable to that of the T-DV-MPCC at both low and high speeds. This highlights the ability of the proposed method to effectively reduce the parameter sensitivity of the T-DV-MPCC method.

Meanwhile, in order to further demonstrate the robustness of the proposed robust method in the full speed range, Fig. 6 shows the current THD of the above two methods in the full speed range, and it can be seen that the phase current THD of the two methods remain similar under the same operating conditions, which again strongly proves the strong robustness of the proposed method.
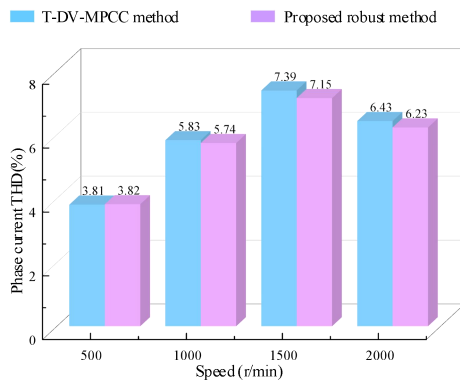

Fig. 7. Comparison of current THD in full speed range between the two methods

6 Conclusions

In order to reduce the dependence of the DV-MPCC method on the motor parameters in the mathematical model, a simple two-vector robust model prediction method is proposed in this paper. The method calculates the set total parameters containing the motor parameter information in real time by constructing the d-axis and q-axis value functions. Then the calculated set total parameter information is used to update and correct the prediction model in real time, and the prediction model can be made infinitely close to the real mathematical model of the motor when it is running, so as to control the motor to run stably and well. Finally, the simulation results verify that the proposed method has good parameter robustness.

7 References

[1] X. Zhang, Y. Cao and C. Zhang, "Model Predictive Voltage Control for PMSM System With Low Parameter Sensitivity," in IEEE Transactions on Industrial Electronics, doi: 10.1109/TIE.2024.3376830.

[2] X. Zhang and Z. Wang, "Simple Robust Model Predictive Current Control for PMSM Drives Without Flux-Linkage Parameter," in IEEE Transactions on Industrial Electronics, vol. 70, no. 4, pp. 3515-3524, April 2023, doi: 10.1109/TIE.2022.3176288.

[3] C. Calleja, A. López-de-Heredia, H. Gaztañaga, L. Aldasoro and T. Nieva, "Validation of a Modified Direct-Self-Control Strategy for PMSM in Railway-Traction Applications," in IEEE Transactions on Industrial Electronics, vol. 63, no. 8, pp. 5143-5155, Aug. 2016.

[4] H. Chaoui and P. Sicard, "Adaptive Fuzzy Logic Control of Permanent Magnet Synchronous Machines With Nonlinear Friction," in IEEE Transactions on Industrial Electronics, vol. 59, no. 2, pp. 1123-1133, Feb. 2012, doi: 10.1109/TIE.2011.2148678.

[5] X. Zhang and Z. Li, "Sliding-Mode Observer-Based Mechanical Parameter Estimation for Permanent Magnet Synchronous Motor," in IEEE Transactions on Power Electronics, vol. 31, no. 8, pp. 5732-5745, Aug. 2016, doi: 10.1109/TPEL.2015.2495183.

[6] S. Li and H. Gu, "Fuzzy Adaptive Internal Model Control Schemes for PMSM Speed-Regulation System," in IEEE Transactions on Industrial Informatics, vol. 8, no. 4, pp. 767-779, Nov. 2012, doi: 10.1109/TII.2012.2205581.

[7] I. Harbi et al., "Model Predictive Control of Multilevel Inverters: Challenges, Recent Advances, and Trends," in IEEE Transactions on Power Electronics, doi: 10.1109/TPEL.2023.3288499.

[8] N. Oikonomou, C. Gutscher, P. Karamanakos, F. D. Kieferndorf and T. Geyer, "Model Predictive Pulse Pattern Control for the Five-Level Active Neutral-Point-Clamped Inverter," in IEEE Transactions on Industry Applications, vol. 49, no. 6, pp. 2583-2592, Nov.-Dec. 2013, doi: 10.1109/TIA.2013.2263273.

[9] L. Xin and Z. Bin, "Sensorless Adaptive Sliding Mode FCS–MPC Using Extended State Observer for PMSM Systerm," 2018 IEEE International Conference of Intelligent Robotic and Control

Engineering (IRCE), Lanzhou, China, 2018, pp. 171-177, doi: 10.1109/IRCE.2018.8492967.

[10] M. Abu-Ali, F. Berkel, M. Manderla, S. Reimann, R. Kennel and M. Abdelrahem, "Deep Learning-Based Long-Horizon MPC: Robust, High Performing, and Computationally Efficient Control for PMSM Drives," in IEEE Transactions on Power Electronics, vol. 37, no. 10, pp. 12486-12501, Oct. 2022, doi: 10.1109/TPEL.2022.3172681.

[11] X. Zhang, Y. Cheng, Z. Zhao and K. Yan, "Optimized Model Predictive Control With Dead-Time Voltage Vector for PMSM Drives," in IEEE Transactions on Power Electronics, vol. 36, no. 3, pp. 3149-3158, March 2021, doi: 10.1109/TPEL.2020.3012985.

[12] Y. Zhang, W. Xie, Z. Li and Y. Zhang, "Low-Complexity Model Predictive Power Control: Double-Vector-Based Approach," in IEEE Transactions on Industrial Electronics, vol. 61, no. 11, pp. 5871-5880, Nov. 2014, doi: 10.1109/TIE.2014.2304935.

[13] N. Jin, M. Chen, L. Guo, Y. Li and Y. Chen, "Double-Vector Model-Free Predictive Control Method for Voltage Source Inverter With Visualization Analysis," in IEEE Transactions on Industrial Electronics, vol. 69, no. 10, pp. 10066-10078, Oct. 2022, doi: 10.1109/TIE.2021.3128905.

[14] F. Wang, L. He and J. Rodriguez, "FPGA-Based Continuous Control Set Model Predictive Current Control for PMSM System Using Multistep Error Tracking Technique," in IEEE Transactions on Power Electronics, vol. 35, no. 12, pp. 13455-13464, Dec. 2020, doi: 10.1109/TPEL.2020.2984336.

[15] C. Ma, J. Rodriguez, C. Garcia and F. De Belie, "Integration of Reference Current Slope Based Model-Free Predictive Control in Modulated PMSM Drives," in IEEE Journal of Emerging and Selected Topics in Power Electronics, vol. 11, no. 2, pp. 1407-1421, April 2023, doi: 10.1109/JESTPE.2022.3159586.

[16] X. Zhang, Z. Zhao, Y. Cheng and Y. Wang, "Robust Model Predictive Current Control Based on Inductance and Flux Linkage Extraction Algorithm," in IEEE Transactions on Vehicular Technology, vol. 69, no. 12, pp. 14893-14902, Dec. 2020, doi: 10.1109/TVT.2020.3043474.